Quaternary Geochronology 35 (2016) 16–25

Contents lists available at ScienceDirect

Quaternary Geochronology

journal homepage: www.elsevier.com/locate/quageo

Research paper

Internal U, Th and Rb concentrations of alkali-feldspar grains: Implications for luminescence dating

R.K. Smedley*, N.J.G. Pearce

Department of Geography and Earth Sciences, Aberystwyth University, Ceredigion, SY23 3DB, UK

ARTICLE INFO

Article history:
Received 18 January 2016
Received in revised form
13 May 2016
Accepted 17 May 2016
Available online 20 May 2016

Keywords:
Luminescence dating
Alkali-feldspar
Internal dose-rate
Uranium
Thorium
Rubidium

ABSTRACT

This study assesses whether internal U, Th and Rb concentrations of single grains of alkali-feldspar can impact upon luminescence dating. Internal alpha dose-rates determined for two sedimentary samples calculated from mean U and Th concentrations accounted for ~10% of the total dose-rates, while internal beta dose-rates from mean Rb concentrations accounted for ~2%. Depth profiles of measurements penetrating into each grain show that internal U and Th concentrations varied between grains, where some grains had effective internal alpha dose-rates up to 1.8 Gy/ka (32% of the total dose-rate). K concentrations inferred from Rb (K_{Rb}) for individual grains suggest that internal U and Th concentrations are related to the feldspar composition. Grains with $K_{Rb} > 6\%$ had low U and Th, and grains with $K_{Rb} < 6\%$ had higher U and Th concentrations. Internal alpha and beta dose-rates of the perthitic and Na-rich grains contaminating the density-separated K-feldspar fractions had a significant impact upon the single-grain D_e distributions, which was estimated to be equivalent to overdispersion values of ~10 − 15%. The scatter in the D_e distributions arising from internal alpha and beta dose-rates for both samples could be reduced by selecting only the brightest 20% of grains for luminescence dating.

1. Introduction

Luminescence dating is a versatile geochronological tool that can directly determine the timing of sediment deposition throughout the Late Quaternary. Two principal minerals are used for luminescence dating: quartz and K-feldspar. A major challenge for luminescence dating of K-feldspar in comparison to quartz is the more complex internal chemistry and crystal structure of feldspar. This is because alkali feldspars form a complete solid solution series under high-temperature magmatic conditions (e.g. in volcanic rocks) between K-rich (sanidine) and Na-rich (high albite) compositions. However, at lower temperatures, an immiscibility gap exists between the Na-rich (low albite) and K-rich (orthoclase, microcline) end-members, which can manifest itself either as perthitic textures or as separate Na- and K-feldspars in plutonic rocks. The presence of K, Rb, U and Th within a feldspar grain provides an internal beta dose-rate, while U and Th also provide an internal alpha dose-rate; thus, it is important that this internal dosimetry is accounted for in the environmental dose-rate used to determine luminescence ages.

Many studies have assessed the internal K-content of single grains of K-feldspar (e.g. Huot and Lamothe, 2012; Neudorf et al., 2012; Smedley et al., 2012; Trauerstein et al., 2014; Gaar et al., 2014) and have shown that some density-separated K-feldspar fractions used for dating can contain perthitic and Na-rich grains. Perthitic structures within alkali feldspar grains form after crystallisation of a homogeneous feldspar by a process of exsolution, where K- and Na-rich areas form within the feldspar to accommodate structural changes in the crystal lattice during cooling. The extent of development of perthitic structures in feldspar is dependent upon the initial K/Na composition of the grain (thus enabling the exsolution of different proportions of K- and Na-rich phases) and history of the crystal (particularly the cooling rate, interaction with aqueous liquids and deformation) (Deer et al., 2013). Where sedimentary samples are dominated by end member feldspar grains, it is easier to perform a physical separation of detrital grains to isolate the K-rich end member for luminescence analysis on the basis of density. However, density separation is more difficult for a sedimentary sample containing perthites (e.g. Smedley et al., 2012). Although detecting the luminescence emission of feldspar grains in blue wavelengths can further isolate the peak emission at ~400 nm of density-separated K-feldspar (Huntley

* Corresponding author.
E-mail address: rks09@aber.ac.uk (R.K. Smedley).

http://dx.doi.org/10.1016/j.quageo.2016.05.002
1871-1014/

et al., 1991), it is possible to detect measurable infra-red stimulated luminescence (IRSL) signals (e.g. Huot and Lamothe, 2012; Smedley et al., 2012; Gaar et al., 2014) and determine equivalent dose (D_e) values (e.g. Huot and Lamothe, 2012; Gaar et al., 2014) from grains which are perthitic or Na-rich. This is because perthitic grains of feldspar have wide emission bands (Prescott and Fox, 1993; Spooner, 1992), and some Na-rich grains that have bright peak emissions in yellow wavelengths can also emit a weaker, but detectable signal in blue wavelengths (e.g. Krbetschek et al., 1997).

The range of partition coefficients published for K-feldspar and plagioclase feldspar show that the uptake of U, Th and Rb during crystallisation leads to lower concentrations of U and Th in K-feldspar than plagioclase feldspar (Table 1 and references therein). Therefore, it is usually assumed that the internal dose-rate of K-rich feldspars will mostly originate from K within the grain and the associated U, Th and Rb contributions are negligible. However, potential exists for perthitic and Na-rich grains to have different concentrations of minor elements (i.e. U, Th and Rb) to the K-rich grains (e.g. Zhao and Li, 2005). Published data of internal U, Th and Rb concentrations within feldspar grains used for luminescence dating are limited, especially for grains of different feldspar compositions. Natural abundances of Rb are suggested to be related to K at a ratio of 270:1 (Mejdahl, 1987) and so any grain-to-grain variability in Rb will likely have a minimal impact upon luminescence dating in comparison to K.

A number of studies have analysed multiple grains of density-separated K-feldspar from sedimentary samples and demonstrated the potential for variability in the internal U and Th concentrations between different samples (Mejdahl, 1987; Duller, 1992) and grains (Zhao and Li, 2005). However, Duller (1992) suggested that effective alpha dose-rates from such samples would be minimal as U and Th concentrations are low in naturally-occurring K-feldspar, and would be located in zones or along cracks within the crystalline structure of the grain (e.g. Mejdahl, 1987). As a consequence, it has become routine practise to either assume a negligible internal alpha dose-rate when calculating environmental dose-rates for K-feldspar (e.g. Duller, 1992; Reimann et al., 2011; Rhodes, 2015), or to apply an internal alpha dose-rate of 0.10 ± 0.05 Gy/ka after Mejdahl (1987) (e.g. Wallinga et al., 2001; Törnqvist et al., 2000; Buylaert et al., 2008, 2011; Sohbati et al., 2012). However, these assumptions may not be appropriate if some of the feldspar grains used to determine ages for some samples are Na-rich or perthitic, or if the grains contain any inclusions (e.g. micron-sized zircon). Internal U, Th and Rb concentrations taken throughout a grain of feldspar used for luminescence dating have not been quantified on a single grain scale. If it was found that significant concentrations of U, Th and Rb were evenly distributed throughout the grain, the effective internal alpha and beta dose-rates would provide a significant contribution to the environmental dose-rate according to concentrations reported for samples in previous studies (e.g. Duller, 1992; Mejdahl, 1987). Therefore, the aim of this study is to quantify internal U, Th and Rb concentrations of K-feldspar grains used for luminescence dating with laser ablation inductively coupled plasma mass spectrometry (LA-ICP-MS) and assess any potential impacts upon ages.

2. Methods

2.1. Sample details

Two sedimentary samples with independent age control were used in this study: sample GDNZ13 and LBA12OW1. Sample GDNZ13 was taken from dune sand from North Island, New Zealand (Duller, 1996) underlying the Kawakawa tephra, which has a radiocarbon age of 25.4 ± 0.2 cal. ka BP (Vandergoes et al., 2013). Sample LBA12OW1 was taken from glaciofluvial sediment associated with the deposition of the Fenix II moraine ridge at Lago Buenos Aires in Patagonia with a terrestrial cosmogenic nuclide (TCN) age of 19.4 ± 1.5 ka (Kaplan et al., 2004, 2011). Luminescence ages for samples GDNZ13 (Smedley, 2014) and LBA12OW1 (Smedley et al., 2016) have previously been published, where the individual grains within the sediments were deemed to have been well bleached prior to burial.

Samples GDNZ13 and LBA12OW1 were chosen for these investigations as the sedimentary samples contain a mixture of end member and perthitic feldspar grains. This is reflected by the intermediate K-contents of the density-separated K-feldspar fractions determined using a 0.1 g sub-sample of the separated material on a Risø GM-25-5 beta counter for samples GDNZ13 (6% K) and LBA12OW1 (5% K). In addition, measurements of the internal K-content of individual grains of samples GDNZ13 (Smedley et al., 2012; Smedley, 2014) and LBA12OW1 (Smedley et al., 2016) have shown the variability between grains in internal K-content, ranging from 0 to 14%. It has been suggested that this variability in internal K-content can explain the relationship between the signal-intensity emitted in response to a fixed test-dose and the D_e values determined for luminescence dating, where K-rich grains emit brighter signals (Reimann et al., 2012; Smedley, 2014; Smedley et al., 2016). Samples GDNZ13 and LBA12OW1 therefore provide an opportunity to assess the variability in internal U, Th and Rb concentrations for grains in a density-separated K-feldspar fraction containing perthites and Na-feldspar due to the nature of the feldspar grains in the source rocks.

2.2. Luminescence dating

2.2.1. Environmental dose-rates

External dose-rates for samples GDNZ13 and LBA12OW1 (Table 2) were determined from milled portions of the bulk sediment using thick source alpha and beta counting on *Daybreak* and *Risø GM-25-5* measurement systems, respectively. Although K-concentrations of 6% (GDNZ13) and 5% (LBA12OW1) were determined for the bulk density-separated K-feldspar fractions, such low K-contents are unlikely to characterise those individual grains used for analysis as K-rich grains are reported to emit brighter IRSL signals when detected in blue wavelengths in comparison to Na-

Table 1
Partition coefficients (Kd) reported for K-feldspar and plagioclase feldspar in the Geochemical Earth Reference Model (GERM) online database. Kd are reported for U (Stix and Gorton, 1990; Nash and Crecraft, 1985), Th (Dudas et al., 1971; Ewart and Griffin, 1994; Bea et al., 1994) and Rb (Luhr and Carmichael, 1980; Mahood and Hildreth, 1983; Nash and Crecraft, 1985; Aignertorres et al., 2007). Typical concentrations of U, Th and Rb in granites are also shown (Faure, 1998) and used to calculate the estimated concentrations of U, Th and Rb in K-feldspar and plagioclase feldspar.

	Range of partition coefficients (Kd)		Typical concentrations of granite (ppm)	Estimated concentrations in grains (ppm)	
	K-feldspar	Plagioclase feldspar		K-feldspar	Plagioclase feldspar
U	0.002 – 0.07	0.05 – 0.13	3	0.0 – 0.2	0.2 – 0.4
Th	0.01 – 0.03	0.004 – 0.382	8.5 – 17	0.1 – 0.5	0.0 – 6.5
Rb	0.11 – 2.85	0.06 – 0.34	110 – 170	12 – 485	7 – 58

Table 2
Environmental dose-rates calculated for coarse-grained (180 – 212 μm) K-feldspar grains in this study using the Dose Rate and Age Calculator (DRAC; Durcan et al., 2015). The water contents used for the calculations in this table were 30 ± 5% (GDNZ13) and 5 ± 2% (LBA12OW1), and the internal K-contents were 10 ± 2%.

Sample	Internal beta dose-rate (Gy/ka)	U (ppm)	Th (ppm)	K (%)	External alpha dose-rate (Gy/ka)	External beta dose-rate (Gy/ka)	External gamma dose-rate (Gy/ka)	Cosmic dose-rate (Gy/ka)	External dose-rate (Gy/ka)	Total dose-rate (Gy/ka)
GDNZ13	0.66 ± 0.12	2.26 ± 0.19	5.25 ± 0.61	1.02 ± 0.07	0.03 ± 0.01	0.83 ± 0.06	0.57 ± 0.04	0.14 ± 0.02	1.56 ± 0.07	2.22 ± 0.14
LBA12OW1	0.66 ± 0.12	2.13 ± 0.25	6.74 ± 0.83	1.83 ± 0.10	0.05 ± 0.01	1.65 ± 0.09	0.96 ± 0.06	0.19 ± 0.02	2.85 ± 0.11	3.51 ± 0.16

rich and perthites (e.g. Krbetschek et al., 1997). Internal K-contents of 12.5 ± 0.5% are routinely applied for dating density-separated K-feldspar fractions after Huntley and Baril (1997). However, an internal K-content of 10 ± 2% was used in this study to calculate the internal beta dose-rate unless otherwise stated after the observations of by Smedley et al. (2012) determined from a more extensive dataset. The dose-rates (Table 2) were calculated using the conversion factors of Guerin et al. (2011), an alpha efficiency value (a-value) of 0.11 ± 0.03 (Balescu and Lamothe, 1993), and alpha (Bell, 1980) and beta (Guerin et al., 2012) dose-rate attenuation factors. The water contents are expressed as a percentage of the mass of dry sediment and were estimated considering the field and saturated water contents, in addition to the environmental history for each sample. Cosmic dose-rates were determined in accordance with Prescott and Hutton (1994).

2.2.2. OSL analysis

To isolate the coarse grains of feldspar for luminescence analysis, the bulk sediment sample was treated with a 10% volume concentration (v/v) dilution of 37% HCl and 20% v/v H_2O_2 to remove carbonates and organics, respectively. Dry sieving was then used to provide the 180 – 212 μm diameter grains, and density-separation using sodium polytungstate and a centrifuge isolated the <2.58 g cm^{-3} (K-feldspar-dominated) fraction. To prevent the non-isotropic removal of the grain surface, the K-feldspar grains were not etched in hydrofluoric acid prior to measurement (Duller, 1992; Porat et al., 2015). The K-feldspar grains were finally mounted into 10 by 10 grids of 300 μm diameter holes in a 9.8 mm diameter aluminium single-grain disc for analysis. All luminescence measurements were performed using a Risø TL/OSL DA-15 automated single-grain system equipped with an infrared laser (830 nm) fitted with an RG-780 filter (3 mm thick) to remove any shorter wavelengths (Bøtter-Jensen et al., 2003; Duller et al., 2003). A blue detection filter pack containing a BG-39 (2 mm), GG-400 (2 mm) and Corning 7–59 (2.5 mm) filter was placed in front of the photomultiplier tube. The system was equipped with a $^{90}Sr/^{90}Y$ beta source delivering ~0.04 Gy/s and the variability of the beta dose given to each hole was found to be negligible (~2%). Each single-grain disc was located at room temperature throughout the sequence rather than the default setting which uses the specified stimulation temperature as this improves the reproducibility of each single-grain measurement (Smedley and Duller, 2013).

A single aliquot regenerative dose (SAR) protocol (Table 3; Murray and Wintle, 2000) was used for determining D_e values for K-feldspar using the post-IR IRSL signal at 225 °C (termed the $pIRIR_{225}$ signal; Thomsen et al., 2008). The IRSL signal was summed over the first 0.3 s of stimulation and the background calculated from the final 0.6 s. Additional uncertainty from the instrument reproducibility of 2.5% (Thomsen et al., 2005; Smedley and Duller, 2013) was incorporated into the calculation of D_e values. Quality control checks were applied and grains were rejected if: (1) the response to the test dose was less than three times the standard deviation of the background; (2) the uncertainty in the luminescence measurement of the test dose was greater than 10%; (3) the recycling ratio was outside the range 0.9 – 1.1, taking into account the uncertainties on the individual ratios; and (4) recuperation was greater than 5% of the response from the largest regenerative dose.

Table 3
Experimental details for the single aliquot regenerative dose (SAR) pIRIR protocol to determine D_e values for individual grains of K-feldspar throughout this study.

Step	Treatment
1	Dose
2	Preheat 250 °C for 60 s
3	SG IRSL 2 s at 60 °C
4	SG IRSL 2 s at 225 °C
5	Test dose (52 Gy)
6	Preheat 250 °C for 60 s
7	SG IRSL 2 s at 60 °C
8	SG IRSL 2 s at 225 °C
9	SG IRSL 3 s at 330 °C

2.3. LA-ICP-MS

LA-ICP-MS analyses (U, Th and Rb) were conducted using a Coherent GeoLas ArF 193 nm Excimer laser coupled to a Thermo Finnegan Element 2 sector field high resolution ICP-MS. Concentrations of U, Th and Rb determined for an ATHO-G reference material using LA-ICP-MS were within error of accepted concentrations published by GeoReM (Table 4). The individual feldspar grains analysed using LA-ICP-MS in this study were kept in the single-grain holders after D_e values were determined for each grain and secured using an organic glue solution (1% PVA) to prevent the grains from moving during ablation. A large beam size with diameter of 80 μm was used for laser ablation at an energy density of 3 J/cm^2, firing at 3 Hz to create an aerosol for analysis using the ICP-MS. Analyses were performed in low mass resolution ($\Delta M/M = 300$) to provide sufficient sensitivity. Table 4 details the detection limits of the elements from LA-ICP-MS analyses. The intensities of the minor elements (determined from the following isotopes: ^{238}U, ^{232}Th, ^{85}Rb) were calibrated by normalisation to ^{29}Si as an internal standard because Si has a near constant stoichiometry within all alkali feldspars. This removes the associated effects of changes in ablation yield between standards and grains, and is standard practise in LA-ICP-MS analysis (see Perkins and Pearce, 1995; Pearce et al., 2004). The NIST-612 glass reference material was used for external calibration (Pearce et al., 1997) by comparing the analyte to ^{29}Si count rates and correcting for the differences in internal standard concentrations between the feldspars and the reference material. For the ICP-MS operating conditions used in this study see Pearce et al. (2011).

To monitor the variability of minor elemental concentrations within individual grains, depth profiles were determined by repeating ablation cycles on the same spot. Between 7 and 10 spectra were acquired from the same crater for each individual grain over a period of 105 – 150 s, this is estimated to have produced craters up to ~150 μm deep and ~80 μm wide in grains of 180

Table 4
Determinations of trace elements in reference material ATHO-G by LA-ICP-MS analyses (ATHO-G data from GeoReM; Jochum et al., 2005 with accepted concentration and 95% confidence limit). The lower limits of detection (LLD) are calculated as three standard deviations on the gas blank, using analyte count rates from the NIST-612 reference material (see Perkins and Pearce, 1995; Pearce et al., 1997). Typical instrument sensitivity is given for these analytical runs as counts per second (cps)/ppm. Averages of analytical error are given for each quartile of determined concentrations in feldspars, calculated from counting statistics as ($cps^{0.5}$/cps) with this ratio then applied to the calculated concentration to give a 1 σ error estimate in the final concentration (Thus for Rb, at concentrations between 190 and 321 ppm (the 3rd quartile), the average 1 σ error is 2.38 ppm, equating to an average relative error (RSD) of 0.99%. As is expected, analytical errors decrease with increasing concentration (see Pearce et al., 2004). The average error for all measurements performed is also given.

		U		Th		Rb
ATHO-G GeoReM accepted values (Jochum et al 2005)						
Accepted ppm		2.37		7.40		65.3
95% C.L. ppm		0.12		0.27		3.0
ATHO-G this study (n = 5)						
Avg. ppm		2.37		7.20		63.5
St. dev. ppm		0.16		0.31		2.3
RSD %		6.8		4.3		3.6
LLD (ppm)		0.00		0.02		0.12
Blank cps ± 1 s.d.		0 ± 0		3 ± 3		~600 ± 20
Typical sensitivity cps/ppm		~1500		~1000		~500
Analytical error estimates	U range (ppm)	U avg. 1 s.d. error, ppm (RSD %)	Th range (ppm)	Th avg. 1 s.d. error, ppm (RSD %)	Rb range (ppm)	Rb avg. 1 s.d. error, ppm (RSD%)
1st quartile	0.004 – 0.10	0.009 (38.2%)	0.02 – 0.27	0.020 (35.5%)	1.16 – 89.7	0.39 (2.40%)
2nd quartile	0.11 – 0.53	0.023 (11.7%)	0.30 – 1.25	0.049 (9.41%)	91.7 – 190	1.58 (1.04%)
3rd quartile	0.65 – 1.77	0.093 (7.97%)	1.66 – 6.46	0.16 (5.32%)	190 – 321	2.38 (0.99%)
4th quartile	1.84 – 3.95	0.14 (5.42%)	6.54 – 32.98	0.29 (2.32%)	324 – 443	3.74 (0.99%)
Avg 1 s.d. for all measurements (ppm)		0.07		0.14		2.02

– 212 μm. Due to the LA-ICP-MS set-up and nature of the analyses, major and minor elements could not be easily and quickly analysed during the same ablation cycle. This restricted the analysis of both K (a major element which requires determination in high mass resolution mode, ΔM/M > 3000; see Smedley et al., 2012) and U, Th and Rb concentrations (minor elements which require determination in low mass resolution mode, ΔM/M = 300) for each individual depth profile. Alternatively, the Rb concentrations were used to infer an approximate K concentration (termed K_{Rb}) using the regression provided from a correlation of Rb with K for 27 feldspar samples, where Rb = −9.17 (ppm) + 38.13 K (%) (Mejdahl, 1987); thus, 28.96 ppm Rb was equivalent to 1% K. This gave an indication as to whether the grain composition was K-rich, Na-rich or perthitic. The mean of the K_{Rb} concentrations determined for single grains from samples GDNZ13 (6%; n = 21 grains) and LBA12OW1 (4%; n = 14 grains) were similar to the respective K-contents of 6 and 5% which were determined for the density-separated fraction of each sample using beta counting (Section 2.1); this improves confidence in the reliability of these estimations of K_{Rb}.

3. Distribution of trace elements within different feldspar grains

Depth profiles determined using LA-ICP-MS assessed the distribution of U and Th within K-feldspar grains used for luminescence dating. The concentrations in the depth profiles determined for grains from sample GDNZ13 (n = 21 grains) and LBA12OW1 (n = 14 grains) demonstrated that the distribution of U and Th varied between individual grains. The grains could be categorised into three types according to the depth profiles (Fig. 1): Type 1 contain low U (<0.1 ppm) and Th (<0.5 ppm) concentrations throughout the depth profile; Type 2 contain high U (>0.5 ppm)

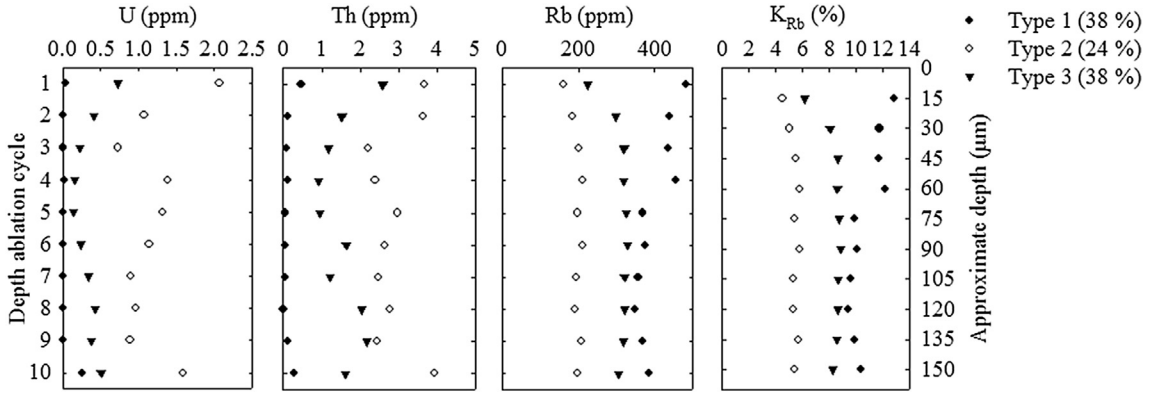

Fig. 1. Examples of depth profiles of internal U, Th, Rb and K_{Rb} concentrations for three different types of grain from sample GDNZ13. Grain types 1, 2 and 3 account for 38%, 24% and 38% of the population, respectively.

and Th (>3 ppm) concentrations throughout the depth profile; and Type 3 contain moderate but variable U (0.1 – 0.5 ppm) and Th (0.5 – 3 ppm) within the depth profile. These depth profiles suggest that the effective internal alpha dose-rates of U and Th will vary between these different grain types.

Comparing the depth profiles of U and Th with the Rb and K_{Rb} concentrations (Fig. 1) provides information on the composition of each feldspar grain. Fig. 1 shows a K-rich (≥10% K_{Rb}) feldspar grain with homogenously low U and Th throughout the depth profile (Type 1), whereas the K_{Rb} concentrations determined for grain Type 2 (6 – 9%) and Type 3 (4 – 6%) are representative of intermediate feldspar, likely with perthitic inclusions. The Type 1 and Type 3 grains (Fig. 1) fulfil the expectations of previous studies that U and Th concentrations of K-feldspar are either low or are variable throughout the grain and so the internal alpha dose rate is less effective. However, the higher U and Th concentrations determined throughout the depth profiles for Type 2 grains suggest that internal alpha dose-rates can contribute significantly to the environmental dose-rate and introduce scatter into single-grain D_e distributions, in addition to the variability caused by the internal beta dose-rate arising from K and Rb.

Mean U, Th and Rb concentrations were then calculated for each depth profile (Fig. 2). The ranges in U, Th and Rb concentrations determined for both samples GDNZ13 and LBA12OW1 are consistent with estimates provided for feldspar grains from reported partition coefficients and typical concentrations in granite (Table 1). Mean Rb concentrations ranged from ~10 ppm to 630 ppm, which suggests that the composition of these feldspar grains was variable. This was also reflected by the K_{Rb} concentrations from 1 – 14% for sample GDNZ13 and 0 – 11% for sample LBA12OW1. A large proportion of the grains had ≤0.4 ppm of U and ≤2 ppm of Th for samples GDNZ13 (81% and 67% of the grains, respectively) and LBA12OW1 (67% and 64% of the grains, respectively). This is similar to reported estimates of U and Th for 16 individual feldspar grains, where 15 out of the 16 grains determined qualitative estimates of U and Th from 0.0 – 0.5 ppm and 0 – 0.6 ppm, respectively, and a single grain in the population had significantly higher respective estimates of 1.4 ppm and 1.7 ppm (Zhao and Li, 2005).

The relationship between the U and Th concentrations and the composition of the feldspar grains was assessed by comparing the mean U, Th and K_{Rb} concentrations determined for each depth profile (Fig. 3). The results show that only one grain categorised as Type 3 had K_{Rb} concentrations >6%. In contrast, the majority of the grains categorised as Type 1 had K_{Rb} concentrations >6%. The comparison between U and Th concentrations and K_{Rb} is consistent with the suggestion that the K-rich end member of the alkali feldspar phase has lower concentrations of U and Th than intermediate feldspar, but higher Rb (Deer et al., 2013). Determining accurate environmental dose-rates will be difficult for a sample that contains K-rich feldspar grains with low internal alpha dose-rates, in addition to perthitic and/or Na-rich feldspar which have a lower K-content, but effective internal alpha dose-rates (i.e. Type 2 grains). Therefore, it is important for single-grain dating of density-separated K-feldspar fractions containing variable K-contents to determine: (1) whether the internal alpha dose-rate can have a significant contribution to the overall dose-rate; (2) whether variability between grains can impact upon the single-grain D_e distributions; and (3) whether the effects of this can be reduced for luminescence dating.

4. Implications for environmental dose-rates

Mean Rb concentrations were calculated from the depth profiles

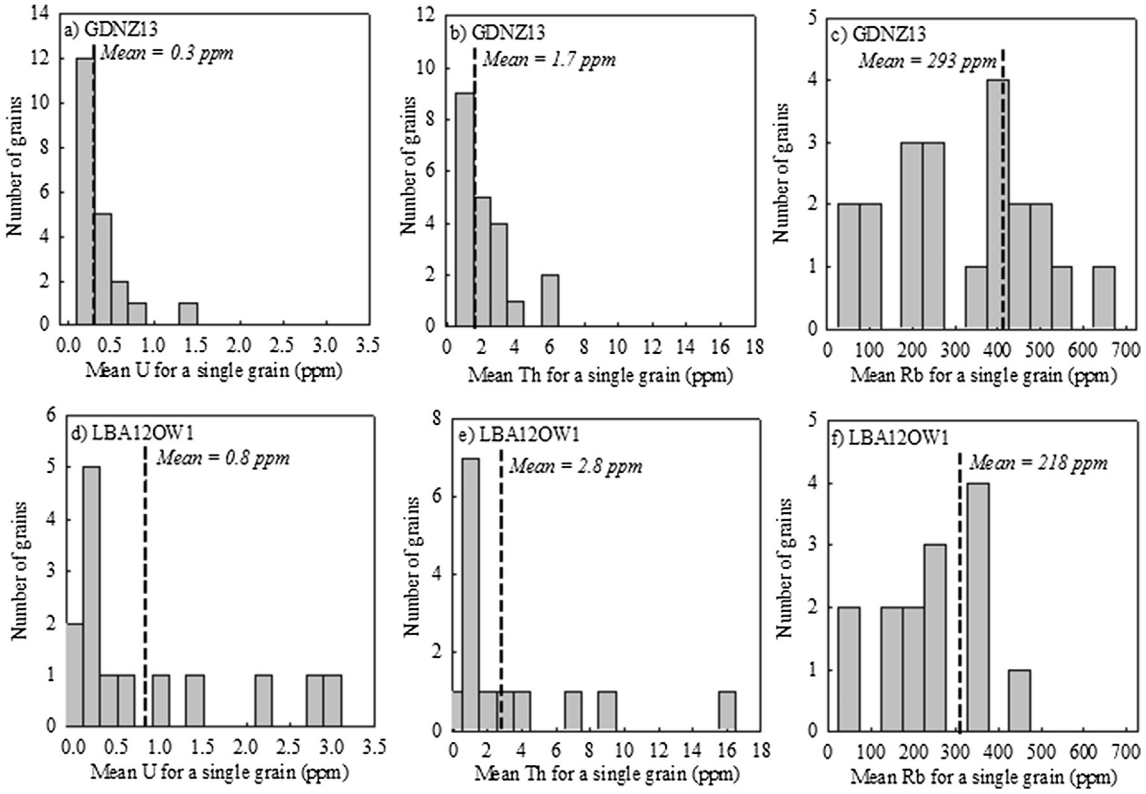

Fig. 2. Histograms of the mean U (a, d), Th (b, e) and Rb (c, f) concentrations calculated from the depth profiles from individual grains from samples GDNZ13 and LBA12OW1 determined using LA-ICP-MS.

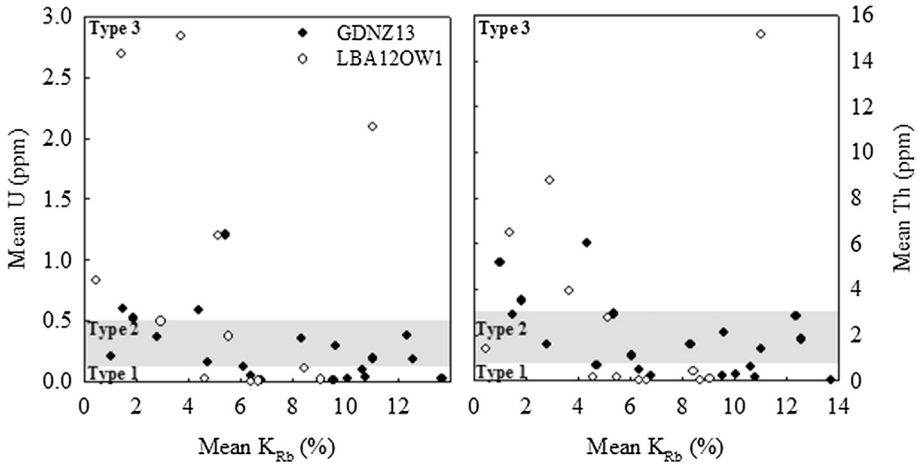

Fig. 3. Internal U and Th concentrations plotted against K_{Rb} concentrations. All values are calculated as means of the depth ablation cycles performed on individual feldspar grains from sample GDNZ13 (n = 21 grains) and LBA12OW1 (n = 14 grains). The grey shading marks the range in U and Th concentrations of Type 2 grains from Fig. 1.

obtained for all of the grains from samples GDNZ13 (293 ppm; Fig. 2c) and LBA12OW1 (218 ppm; Fig. 2f) and equate to an internal beta dose-rate of 0.07 ± 0.01 Gy/ka and 0.06 ± 0.01 Gy/ka, respectively. These internal beta dose-rates from Rb are similar to those determined for a variety of sedimentary samples from multiple grains (e.g. Mejdahl, 1987) and account for a similarly small proportion of the total dose-rate (i.e. from 1 – 4%). While Rb can provide an internal beta dose-rate during burial of the grains, it is low in comparison to the internal beta dose-rate from K.

Mean internal U and Th concentrations were also calculated from the depth profiles determined for the grains analysed from samples GDNZ13 (U 0.3 ppm, Th 1.7 ppm) and LBA12OW1 (U 0.8 ppm, Th 2.8 ppm) (Fig. 2). The U and Th concentrations were broadly consistent with semi-quantitative estimates ranging from 0.2 – 0.5 ppm for U and 1.7 – 3.0 ppm for Th which were determined for samples of similar material to GDNZ13 from dune sand in New Zealand using a spiked internal standard for calibration (Duller, 1992). Internal alpha and beta dose-rates were then calculated for samples GDNZ13 (U 0.3 ppm, Th 1.7 ppm) and LBA12OW1 (U 0.8 ppm, Th 2.8 ppm) using the mean U and Th concentrations determined from LA-ICP-MS analysis and assuming an internal K-content of 10 ± 2% (see Section 2.2.1). When combining the beta dose-rate arising from U and Th with that from K, the internal beta dose-rates for samples GDNZ13 (0.68 ± 0.12 Gy/ka) and LBA12OW1 (0.70 ± 0.12 Gy/ka) increased by 3% and 6% respectively from the internal beta dose-rate determined using only the internal K-content of 10 ± 2% (0.66 ± 0.12 Gy/ka). The internal alpha dose-rates arising solely from U and Th inside the grain were 0.22 ± 0.04 and 0.45 ± 0.07 Gy/ka for samples GDNZ13 and LBA12OW1, respectively. These internal alpha dose-rates are similar to those previously determined for sedimentary samples used for luminescence dating (e.g. Kolstrup and Mejdahl, 1986; Mejdahl, 1992; Edwards, 1993) and suggest that it may not be appropriate to assume an internal alpha dose-rate of 0.10 ± 0.05 Gy/ka (after Mejdahl, 1987) for luminescence dating of these samples when all of the grains are used to determine a D_e value.

The proportion of the overall dose-rate (Section 2.2.1) for each component has been calculated when the contributions from internal U and Th are included with the calculations in Table 2 (Fig. 4). The external dose-rates account for a large proportion of the total dose-rates for samples GDNZ13 (64%) and LBA12OW1 (71%), respectively. The majority of the internal dose-rate arises from beta

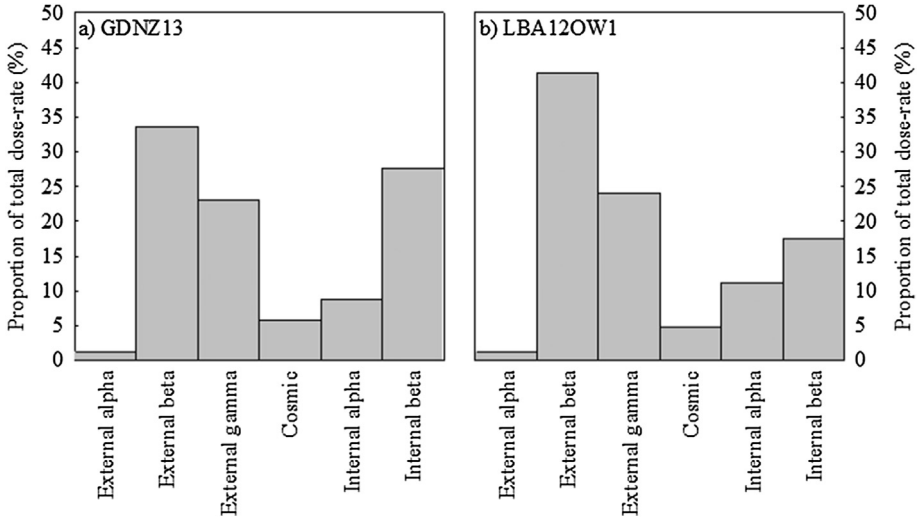

Fig. 4. Proportions of the total dose-rate from the different sources of dosimetry. The internal alpha and beta dose-rates were calculated using an internal K-content for both samples of 10 ± 2% and the mean internal U and Th concentrations determined using LA-ICP-MS for each sample.

provided by K and Rb within the grain: 28% of the total dose-rate for GDNZ13 and 18% for LBA12OW1. However, based on the LA-ICP-MS analyses in this study, the mean internal alpha dose-rates determined for samples GDNZ13 and LBA12OW1 account for 9% and 11% of the total dose-rates, respectively (Fig. 4). This contribution is larger than the external alpha dose-rate and the cosmic dose-rate for both samples; both of these contributions are routinely accounted for when calculating environmental dose-rates for luminescence dating. It is therefore important to address the contributions of internal alpha dose-rates arising from U and Th within the grains, especially given the potential for large variability between different grains for samples containing variable types of feldspar grains.

5. Impact upon luminescence characteristics

To assess whether luminescence dating of K-feldspar from samples GDNZ13 and LBA12OW1 could be affected by the analysis of grains with variable internal U and Th concentrations, the internal dosimetry of each individual grain from sample GDNZ13 and LBA12OW1 is compared with the D_e value determined for dating (Fig. 5). Previous studies have suggested that the variability in internal K-content for both samples GDNZ13 (Smedley, 2014) and LBA12OW1 (Smedley et al., 2016) can be reduced by selecting the brightest 20% of grains for luminescence dating. For sample GDNZ13 and LBA12OW1, this included the grains that emitted signal-intensities in response to a fixed 52 Gy test-dose of

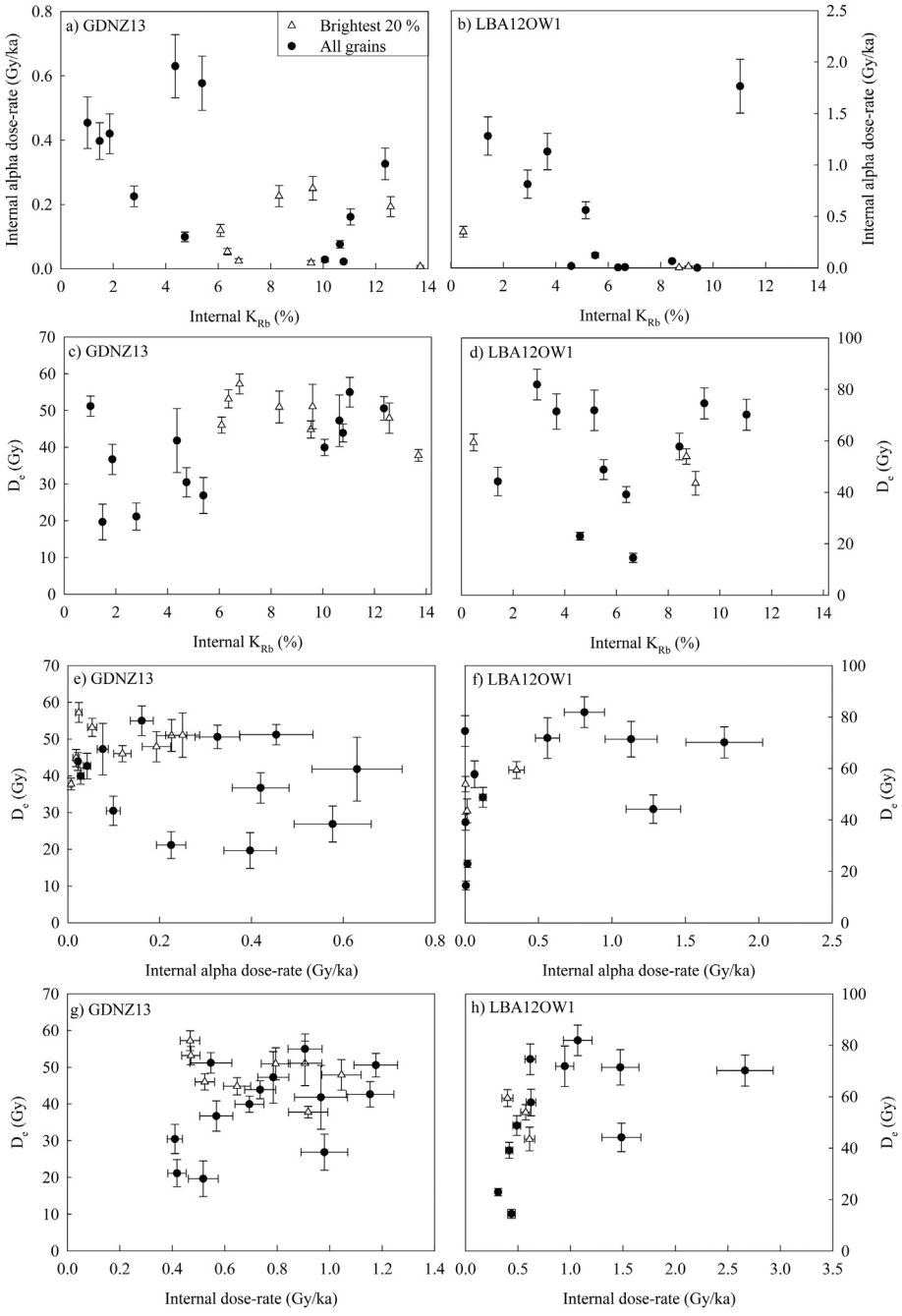

Fig. 5. Comparing the results determined from geochemical and luminescence analyses.

>10,000 cts/0.3 s and >4000 cts/0.3 s, respectively. The grains used for geochemical analysis in this study were taken as a subsample of the dataset used for luminescence dating of both these samples and so the sub-sampled grains could be categorised into those grains that were part of the brightest 20% of the population and those that were not (Fig. 5). A total of eight out of the 21 grains for sample GDNZ13 were categorised as the brightest grains (e.g. Fig. 5a), whereas only three out of the total 14 grains were categorised as the brightest grains for sample LBA12OW1 (e.g. Fig. 5b).

5.1. Feldspar composition

Internal alpha dose-rates are compared to the K_{Rb} concentrations for samples GDNZ13 (Fig. 5a) and LBA12OW1 (Fig. 5b). For sample GDNZ13, the results suggest that the larger internal alpha dose-rates (≥0.4 Gy/ka) were determined from grains with K_{Rb} concentrations that are <6%, and that these grains were not part of the brightest 20% of the grains. Moreover, by selecting only the brightest 20% of the grains for sample GDNZ13, the range in internal alpha dose-rate was reduced from 0 − 0.63 Gy/ka for all grains to 0 − 0.25 Gy/ka. Larger internal alpha dose-rates (>0.25 Gy/ka) were also determined for the grains of sample LBA12OW1 that had K_{Rb} concentrations of <6%. However, one grain was an exception to this trend as it had ~11% K_{Rb} and an internal alpha dose-rate of ~1.7 Gy/ka. The range in internal alpha dose-rates reduced from 0 − 1.8 Gy/ka for all grains to 0 − 0.35 Gy/ka when only the brightest 20% of grains were selected from sample LBA12OW1. The results shown in Fig. 5 for both samples provide evidence to suggest that previous studies (Smedley, 2014; Smedley et al., 2016) have reduced the variability between grains in internal K-contents and reduced the influence of internal alpha dose-rates upon luminescence dating by selecting the brightest 20% of grains for both samples GDNZ13 and LBA12OW1.

5.2. Internal K-contents

The geochemical data determined in this study provide a rare opportunity to determine internal alpha and beta dose-rates arising from K_{Rb}, U and Th for grains that are used to determine D_e values for dating. If either or both internal dose-rates have a dominant control on the D_e distributions, it is expected that there will be a relationship between the two parameters. The K_{Rb} concentrations determined for each grain from samples GDNZ13 (Fig. 5c) and LBA12OW1 (Fig. 5d) have been compared with the corresponding D_e values used for dating. The results show that there is a broad positive relationship approaching significance ($R = 0.41$ with $p = 0.06$) between K_{Rb} concentrations and D_e values for all the individual grains from sample GDNZ13 (Fig. 5c). An R value of 0.41 ($p = 0.06$) suggests that the internal K-content is likely to have had a control on the single-grain D_e distribution for this sample. However, for sample LBA12OW1 there is no relationship ($R = 0.02$ with $p = 0.94$) between the D_e values and K_{Rb} (Fig. 5d). This difference between the data shown for GDNZ13 (Fig. 5c) and LBA12OW1 (Fig. 5d) may be related to the fact that the internal dose-rate accounts for a smaller proportion of the total dose-rate for sample LBA12OW1 (17%) in comparison to GDNZ13 (28%) and/or the larger contributions provided by the internal alpha dose-rate for sample LBA12OW1 (Fig. 5b) in comparison to sample GDNZ13 (Fig. 5a). Unfortunately, the datasets for the brightest 20% of the grains for both samples are too small to provide a reliable assessment of any relationship between D_e and K_{Rb}.

5.3. Internal alpha dose-rates

The internal alpha dose-rates arising from U and Th have also been compared to the D_e values determined for individual grains of both sample GDNZ13 (Fig 5e) and LBA12OW1 (Fig 5f). Any direct relationship between internal alpha dose-rates and D_e values for these samples is difficult to identify because of the large uncertainties determined for some of the grains. However, the grains with large uncertainties in the D_e values also determine larger internal alpha dose-rates, and are the dimmer grains in the D_e distribution. Fig. 5e suggests that it is beneficial to select the brightest 20% of grains as it reduces the impact of those grains on the single-grain D_e distribution, which have large internal alpha dose-rates and determine variable D_e values.

5.4. Combined internal alpha and beta dose-rates

The internal alpha and beta dose-rates are then combined for each grain of samples GDNZ13 (Fig. 5g) and LBA12OW1 (Fig. 5h) and compared with the corresponding D_e values. The data suggests that there is no direct relationship between the internal dose-rates and D_e values for sample GDNZ13 (Fig. 5g) or LBA12OW1 (Fig. 5h). This is likely because other factors also contribute towards the scatter in a single-grain D_e distribution determined for K-feldspar. For example, variability in the external dose-rate received by each individual grain (i.e. external microdosimetry) may have caused additional scatter in the single-grain D_e distributions as 64% (GDNZ13) and 70% (LBA12OW1) of the total dose-rate originates from the external dose-rate. Variability between grains in factors inherent to the analysis of single grains of feldspar using the pIRIR signal may also have contributed towards the scatter in single-grain D_e distributions (e.g. bleaching rate of the pIRIR signal and anomalous fading). Given that a number of different factors influence the scatter in a single-grain D_e distribution determined for K-feldspar, it is unlikely that a single factor will have a direct relationship with the D_e values; this is reflected in the comparison with the internal alpha and beta dose-rates presented here.

6. Implications for luminescence dating

6.1. Simulated D_e distributions

The independent age control provided for the well-bleached samples GDNZ13 (radiocarbon dating) and LBA12OW1 (TCN dating) provides an opportunity to assess the influence of internal dose-rates on the scatter in single-grain D_e distributions. Grain-specific environmental dose-rates have been calculated in three different ways using the external dose-rates (Table 2) and geochemical data determined from LA-ICP-MS: (1) using K_{Rb} and Rb concentrations and excluding internal U and Th; (2) using an assumed internal K-content of 10 ± 2% and the measured internal U and Th concentrations; and (3) using combined internal dose-rates derived from K_{Rb}, Rb, U and Th. These grain-specific dose-rates were then multiplied by the independent age control to determine the expected D_e value for each grain, which in turn simulated single-grain D_e distributions that are the result of internal dose-rates.

Overdispersion values of 11 ± 1% (applying internal K_{Rb} and Rb and excluding internal U and Th), 8 ± 1% (applying an assumed internal K-content of 10 ± 2% and the measured internal U and Th) and 10 ± 1% (combining internal dose-rates from K_{Rb}, Rb, U and Th) were determined from these D_e distributions for sample GDNZ13. The simulated single-grain D_e distributions suggest that variability caused by internal K_{Rb} and Rb (~11%) caused similar scatter in the D_e distribution to the internal alpha dose-rates (~8%) for sample GDNZ13. The single-grain D_e distributions simulated from the combined internal alpha and beta dose-rates (~10%) suggest that the internal alpha dose-rates counter-balance some of the scatter

Table 5
Results from LA-ICP-MS analyses and luminescence dating for the samples in this study.

	Mean internal alpha dose-rate (Gy/ka)	Adjusted dose-rate (Gy/ka)	n	CAM D_e (Gy)	Age (ka)
GDNZ13 25.4 ± 0.2 cal ka BP					
All grains	0.2	2.42 ± 0.14	597	44.2 ± 0.5	18.3 ± 1.1
Brightest	0.1	2.34 ± 0.14	119	50.5 ± 0.7	21.6 ± 1.3
LBA12OW1 19.4 ± 1.5 ka					
All grains	0.4	3.91 ± 0.16	179	58.1 ± 1.8	14.9 ± 0.8
Brightest	0.1	3.61 ± 0.16	36	61.2 ± 2.8	17.0 ± 1.1

caused by the internal beta dose-rates as those grains with larger internal alpha dose-rates had lower internal beta dose-rates. For sample LBA12OW1, overdispersion values of 9 ± 1% (applying internal K_{Rb} and Rb and excluding internal U and Th), 15 ± 1% (applying an assumed internal K-content of 10 ± 2% and the measured internal U and Th) and 15 ± 1% (combining internal dose-rates from K_{Rb}, Rb, U and Th) were determined for the simulated D_e distributions. The overdispersion values suggest that internal alpha dose-rates cause more scatter (~15%) than the internal beta dose-rates (~9%) for sample LBA12OW1.

The overdispersion values determined for the simulated D_e distributions could then be related to the natural D_e distributions by comparison with the overdispersion values provided from the original studies of samples GDNZ13 (Smedley, 2014) and LBA12OW1 (Smedley et al., 2016), which were 25 ± 1% and 39 ± 1%, respectively. When only the brightest 20% of these grains from GDNZ13 (14 ± 1%) and LBA12OW1 (26 ± 1%) were used to determine overdispersion, the values were lower. This is consistent with the suggestion that selecting the brighter grains better isolates the K-rich feldspar grains, and the overdispersion values of 10 ± 1% (GDNZ13) and 15 ± 1% (LBA12OW1) determined from the single-grain D_e distribution simulated using the internal alpha and beta dose-rates can explain the reduction in scatter. Understanding the amount of scatter in a D_e distribution caused by internal dose-rates of K-feldspar is important as it can inform the parameters that should be used for statistical modelling (e.g. σ_b in the minimum age model) of single-grain D_e distributions determined from heterogeneously-bleached sediments.

6.2. Natural D_e distributions used for luminescence dating

Mean internal alpha dose-rates were calculated for all the grains analysed using LA-ICP-MS, in addition to only those categorised as the brightest 20% of the grains from Section 5 (Table 5). Although the datasets for the brightest grains of sample GDNZ13 (n = 8 grains) and LBA12OW1 (n = 3 grains) are small, comparing the brighter and dimmer grains gives an indication of the potential differences in geochemistry between them. The mean internal alpha dose-rate for sample GDNZ13 reduced from ~0.2 Gy/ka (all grains; 9% of the total dose-rate) to ~0.1 Gy/ka (brightest 20% of grains; 5% of the total dose-rate), and from ~0.4 Gy/ka (all grains; 11% of the total dose-rate) to ~0.1 Gy/ka (brightest 20% of grains; 9% of the total dose-rate) for sample LBA12OW1. The environmental dose-rates for both samples from Table 2 have been adjusted to include the approximate internal alpha dose-rates for all the grains, in addition to only the brightest 20% of the grains (Table 5). The CAM D_e values provided from the original studies for samples GDNZ13 (Smedley, 2014) and LBA12OW1 (Smedley et al., 2016) have been divided by the adjusted dose-rates to calculate new ages (Table 5). The age determined from only the brightest 20% for sample LBA12OW1 still agrees within ±1σ with the independent age control for sample LBA12OW1 (Table 5). However, the age determined for only the brightest 20% of grains still underestimates the independent age control beyond ±2σ. Underestimation of pIRIR ages by ~10% determined when using only the brightest 20% of the feldspar grains in comparison to independent age control was identified by the original study (Smedley, 2014) and have also been reported by other studies (e.g. Reimann et al., 2012). At present it is unknown what causes this underestimation, but the geochemical analyses in this study suggest that it cannot be explained by the internal dose-rate.

7. Conclusions

Geochemical analyses of U, Th and Rb using LA-ICP-MS in this study have provided unique insights into the internal dosimetry of single grains of feldspar used for luminescence dating. Depth profiles of LA-ICP-MS ablation cycles penetrating through each grain of feldspar showed that the distribution of U and Th within the grains could be characterised into three types: Type 1 had low U (<0.1 ppm) and Th (<0.5 ppm); Type 2 had high U (>0.5 ppm) and Th (>3.0 ppm); and Type 3 had moderate but variable U (0.1 − 0.5 ppm) and Th (0.5 − 3.0 ppm). The depth profiles suggested that effective internal alpha dose-rates from U and Th of these different grain types will likely vary, with Type 2 grains receiving a significant internal alpha dose-rate which is not restricted to zones within the crystal structure.

Comparing mean internal U and Th concentrations calculated from the depth profiles of each grain with internal K_{Rb} concentrations suggests that the variability in U and Th is linked with the feldspar composition (i.e. K-rich, Na-rich or perthitic). The majority of K-rich feldspar grains were characterised by lower internal alpha dose-rates (<0.4 Gy/ka), and the grains with <6% K_{Rb} had larger internal alpha dose-rates (>0.4 Gy/ka). Variability between grains of internal dose-rates will therefore have a minimal impact upon single-grain D_e distributions obtained from sedimentary samples containing only K-feldspar that are easily separated on the basis of density. However, grain-to-grain variability in internal dose-rates will incorporate more scatter into D_e distributions obtained from density-separated K-feldspar fractions contaminated by Na-rich and perthitic grains. Single-grain D_e distributions simulated using independent age control and grain-specific dose-rates determined from the LA-ICP-MS data suggest that overdispersion values of ~10% and ~15% could be explained by internal dose-rates of feldspar. The geochemical evidence in this study suggests that it is important to select only the brightest 20% of grains from density-separated K-feldspar fractions that are contaminated by Na-rich or perthitic grains to circumvent the scatter in single-grain D_e distributions that is potentially caused by grain-to-grain variability in internal dose-rates used for luminescence dating.

Acknowledgments

Financial support for the work contributing towards this paper was provided by a NERC PhD studentship to RKS (NE/I1527845/1). G. Duller is thanked for providing the aeolian dune sand from New Zealand (GDNZ13) and N. Glasser is acknowledged for the field assistance when collecting sample LBA12OW1 in Argentine

Patagonia. A. Brown is thanked for providing the adhesive solution for this work and J. Durcan is thanked for initial feedback on this manuscript. The authors would like to thank an anonymous reviewer and K. Ramseyer for their constructive comments on this manuscript.

References

Aignertorres, M., Blundy, J., Ulmer, P., Pettke, T., 2007. Laser Ablation ICPMS study of trace element partitioning between plagioclase and basaltic melts: an experimental approach. Contrib. Mineral. Petrol. 153, 647–667.

Balescu, S., Lamothe, M., 1993. Thermoluminescence dating of the holsteinian marine formation of Herzeele, northern France. J. Quat. Sci. 8, 117–124.

Bea, F., Pereira, M.D., Stroh, A., 1994. Mineral/leucosome trace-element partitioning in a peraluminous migmatite (a laser ablation-ICP-MS study). Chem. Geol. 117, 291–312.

Bell, W.T., 1980. Alpha dose attenuation in quartz grains for thermoluminescence dating. Anc. TL 12, 4–8.

Bøtter-Jensen, L., Andersen, C.E., Duller, G.A.T., Murray, A.S., 2003. Developments in radiation, stimulation and observation facilities in luminescence measurements. Radiat. Meas. 37, 535–541.

Buylaert, J.-P., Murray, A.S., Huot, S., 2008. Optical dating of an Eemian site in Northern Russia using K-feldspar. Radiat. Meas. 43, 715–720.

Buylaert, J.-P., Huot, S., Murray, A.S., Van Den Haute, P., 2011. Infrared stimulated luminescence dating of an Eemian (MIS 5e) site in Denmark using K-feldspar. Boreas 40, 46–56.

Deer, W.A., Howie, R.A., Zussman, J., 2013. An Introduction to the Rock-forming Minerals, third ed. Berforts Information Press, Hertfordshire, U.K.

Duller, G.A.T., 1992. Luminescence Chronology of Raised Marine Terraces Southwest North Island New Zealand. Unpublished PhD thesis. University of Wales, Aberystwyth.

Duller, G.A.T., 1996. The age of the Koputaroa dunes, southwest North Island, New Zealand. Palaeogeogr. Palaeoclimatol. Palaeoecol. 121, 105–114.

Duller, G.A.T., Bøtter-Jensen, L., Murray, A.S., 2003. Combining infrared- and green-laser stimulation sources in single-grain luminescence measurements of feldspar and quartz. Radiat. Meas. 37, 543–550.

Dudas, M.J., Schmitt, R.A., Harward, M.E., 1971. Trace element partitioning between volcanic plagioclase and dacitic pyroclastic matrix. Earth Planet. Sci. Lett. 11, 440–446.

Durcan, J.A., King, G.E., Duller, G.A.T., 2015. DRAC: dose rate and age calculator for trapped charge dating. Quat. Geochronol. 28, 54–61.

Edwards, S.R., 1993. Luminescence Dating of Sand from the Kelso Dunes, California. In: Geological Society, London, Special Publications, 72, pp. 59–68.

Ewart, A., Griffin, W.L., 1994. Application of proton-microprobe data to trace-element partitioning in volcanic-rocks. Chem. Geol. 117, 251–284.

Faure, G., 1998. Principles and Applications of Geochemistry: a Comprehensive Textbook for Geology Students. Prentice Hall, UK.

Gaar, D., Lowick, S.E., Preusser, F., 2014. Performance of different luminescence approaches for the dating of known-age glaciofluvial deposits from northern Switzerland. Geochronometria 41, 65–80.

Geochemical Earth Reference Model (GERM) online database, www.earthref.org, 2016.

Guerin, G., Mercier, N., Adamiec, G., 2011. Dose-rate conversion factors: update. Anc. TL 29, 5–8.

Guerin, G., Mercier, N., Nathan, R., Adamiec, G., Lefrais, Y., 2012. On the use of the infinite matrix assumption and associated concepts: a critical review. Radiat. Meas. 47, 778–785.

Huntley, D.J., Baril, M.R., 1997. The K-content of the K-feldspars being measured in optical dating or in thermoluminescence dating. Anc. TL 15, 11–13.

Huntley, D.J., Godfrey-Smith, D.I., Haskell, E.H., 1991. Light-induced emission spectra from some quartz and feldspars. Nucl. Tracks Radiat. Meas. 18, 127–131.

Huot, S., Lamothe, M., 2012. The implication of sodium-rich plagioclase minerals containing K-rich feldspars aliquots in luminescence dating. Quat. Geochronol. 10, 334–339.

Jochum, K.P., Nohl, U., Herwig, K., Lammel, E., Stoll, B., Hofmann, A.W., 2005. GeoRem: a new geochemical database for reference materials and isotopic standards. Geostand. Geoanalytical Res. 29, 333–338.

Kaplan, M.R., Ackert, R.P., Singer, B.S., Douglass, D.C., Kurz, M.D., 2004. Cosmogenic nuclide chronology of millennial-scale glacial advances during O-Isotope stage 2 in Patagonia. Geol. Soc. Am. Bull. 116, 308–321.

Kaplan, M.R., Strelin, J.A., Schaefer, J.M., Denton, G.H., Finkel, R.C., Schwartz, R., Putnam, A.E., Vandergoes, M.J., Goehring, B.M., Travis, S.G., 2011. In-situ cosmogenic ^{10}Be production rate at Lago Argentino, Patagonia: implications for late-glacial climate chronology. Earth Planet. Sci. Lett. 309, 21–32.

Krbetschek, M.R., Götze, J., Dietrich, A., Trautmann, T., 1997. Spectral information from minerals relevant for luminescence dating. Radiat. Meas. 27, 695–748.

Kolstrup, E., Mejdahl, V., 1986. Three frost wedge casts from Jutland (Denmark) and TL dating of their infill. Boreas 15, 311–321.

Luhr, J.F., Carmichael, I.S.E., 1980. The Colima volcanic complex, Mexico. I: post-caldera andesites from Volcan Colima. Contributions Mineralogy Petrology 71, 343–372.

Mahood, G.A., Hildreth, E.W., 1983. Large partition coefficients for trace elements in high-silica rhyolites. Geochim. Cosmochim. Acta 47, 11–30.

Mejdahl, V., 1987. Internal radioactivity in quartz and feldspar grains. Anc. TL 5, 10–17.

Mejdahl, V., 1992. Thermoluminescence dating of late-glacial sand sediments. Nucl. Tracks Radiat. Meas. 18, 71–75.

Murray, A.S., Wintle, A.G., 2000. Luminescence dating of quartz using an improved single-aliquot regenerative-dose protocol. Radiat. Meas. 32, 57–73.

Nash, W.P., Crecraft, H.R., 1985. Partition coefficients for trace elements in silicic magmas. Geochim. Cosmochim. Acta 49, 2309–2322.

Neudorf, C.M., Roberts, R.G., Jacobs, Z., 2012. Sources of overdispersion in a K-rich feldspar sample from north-central India: insights from D_e, K content and IRSL age distributions for individual grains. Radiat. Meas. 47, 696–702.

Pearce, N.J.G., Perkins, W.T., Westgate, J.A., Gorton, M.P., Jackson, S.E., Neal, C.R., Chenery, S.P., 1997. A compilation of new and published major and trace element data for NIST SRM 610 and NIST SRM 612 glass reference materials. Geostand. Newsl. 21, 115–144.

Pearce, N.J.G., Westgate, J.A., Perkins, W.T., Preece, S.J., 2004. The application of ICP-MS methods to tephrochronological problems. Appl. Geochem. 19, 289–322.

Pearce, N.J.G., Perkins, W.T., Westgate, J.A., Wade, S.C., 2011. Trace-element microanalysis by LA-ICP-MS: the quest for comprehensive chemical characterisation of single, sub-10 μm volcanic glass shards. Quat. Int. 246, 57–81.

Perkins, W.T., Pearce, N.J.G., 1995. Mineral microanalysis by laserprobe inductively coupled plasma mass spectrometry. In: Potts, P.J., Bowles, J.F.W., Reed, S.J.B., Cave, M.R. (Eds.), Microprobe Techniques in the Earth Sciences. The Mineralogical Society, pp. 291–325.

Porat, N., Faerstein, G., Medialdea, A., Murray, A., 2015. Re-examination of common extraction and purification methods of quartz and feldspar for luminescence dating. Anc. TL 33 (1), 22–30.

Prescott, J.R., Fox, P.J., 1993. Three-dimensional thermoluminescence spectra of feldspars. J. Phys. D Appl. Phys. 26, 2,245–2,254.

Prescott, J.R., Hutton, J.T., 1994. Cosmic ray and gamma ray dosimetry for TL and ESR. Nucl. Tracks Radiat. Meas. 14, 223–227.

Reimann, T., Tsukamoto, S., Naumann, M., Frechen, M., 2011. The potential of using K-rich feldspars for optical dating of young coastal sediments – a test case from Darss-Zingst peninsula (southern Baltic Sea coast). Quat. Geochronol. 6, 207–222.

Reimann, T., Thomsen, K.J., Jain, M., Murray, A.S., Frechen, M., 2012. Single-grain dating of young sediment using the pIRIR signal from feldspar. Quat. Geochronol. 11, 28–41.

Rhodes, E.J., 2015. Dating sediments using potassium feldspar single-grain IRSL: initial methodological considerations. Quat. Int. 362, 14–22.

Smedley, R.K., Glasser, N.F., Duller, G.A.T., 2016. Luminescence dating of glacial advances at Lago Buenos Aires (~46 °S), Patagonia. Quat. Sci. Rev. 134, 59–73.

Smedley, R.K., 2014. Testing the Use of Single Grains of K-feldspar for Luminescence Dating of Proglacial Sediments in Patagonia. Ph.D thesis. Aberystwyth University, U.K.

Smedley, R.K., Duller, G.A.T., 2013. Optimising the reproducibility of measurements of the post-IR IRSL signal from single-grains of feldspar for dating. Anc. TL 31 (2), 49–58.

Smedley, R.K., Duller, G.A.T., Pearce, N.J.G., Roberts, H.M., 2012. Determining the K-content of single-grains of feldspar for luminescence dating. Radiat. Meas. 47, 790–796.

Sohbati, R., Murray, A.S., Buylaert, J.-P., Ortuño, M., Cunha, P.P., Masana, E., 2012. Luminescence dating of Pleistocene alluvial sediments affected by the Alhama de Murcia fault (eastern Betics, Spain) – a comparison between OSL, IRSL and post-IR IRSL ages. Boreas 41, 250–262.

Spooner, N.A., 1992. Optical dating: preliminary results on the anomalous fading of luminescence from feldspars. Quat. Sci. Rev. 11, 139–145.

Stix, J., Gorton, M.P., 1990. Variations in trace-element partition-coefficients in sanidine in the cerro toledo rhyolite, jemez mountains, New-Mexico - effects of composition, temperature, and volatiles. Geochim. Cosmochim. Acta 54, 2,697–2,708.

Törnqvist, T.E., Wallinga, J., Murray, A.S., de Wolf, H., Cleveringa, P., de Gans, W., 2000. Response of the Rhine-Meuse system (west-central Netherlands) to the last Quaternary glacio-eustatic cycles: a first assessment. Glob. Planet. Change 27, 89–111.

Thomsen, K.J., Murray, A.S., Botter-Jensen, L., 2005. Sources of variability in OSL dose measurements using single grains of quartz. Radiat. Meas. 39, 47–61.

Thomsen, K.J., Murray, A.S., Jain, M., Bøtter-Jensen, L., 2008. Laboratory fading rates of various luminescence signals from feldspar-rich sediment extracts. Radiat. Meas. 43, 1474–1486.

Trauerstein, M., Lowick, S.E., Preusser, F., Schulunegger, F., 2014. Small aliquot and single grain IRSL and post-IR IRSL dating of fluvial and alluvial sediments from the Pativilca valley. Peru. Quat. Geochronol. 22, 163–174.

Vandergoes, M.J., Hogg, A.G., Lowe, D.J., Newnham, R.M., Denton, G.H., Southon, J., Barrell, D.J.A., Wilson, C.J.N., McGlone, M.S., Allan, A.S.R., Almond, P.C., Pletchey, F., Dabell, K., Dieffenbacher-Krall, A.C., Blaauw, M., 2013. A revised age for the Kawakawa/Oruanui tephra, a key marker for the Last Glacial Maximum in New Zealand. Quat. Sci. Rev. 74, 195–201.

Wallinga, J., Murray, A.S., Duller, G.A.T., Törnqvist, T.E., 2001. Testing optically stimulated luminescence dating of sand-sized quartz and feldspar from fluvial deposits. Earth Planet. Sci. Lett. 193, 617–630.

Zhao, H., Li, S.H., 2005. Internal dose rate to K-feldspar grains from radioactive elements other than potassium. Radiat. Meas. 40, 84–93.